Regulatory module involving FGF13, miR-504, and p53 regulates ribosomal biogenesis and supports cancer cell survival

Débora R. Bublik[a], Slađana Bursać[b], Michal Sheffer[c,1], Ines Oršolić[b], Tali Shalit[d], Ohad Tarcic[a], Eran Kotler[a], Odelia Mouhadeb[a,2], Yonit Hoffman[a], Gilad Fuchs[a], Yishai Levin[d], Siniša Volarević[b], and Moshe Oren[a,3]

[a]Department of Molecular Cell Biology, Weizmann Institute of Science, Rehovot 76100, Israel; [b]Department of Molecular Medicine and Biotechnology, School of Medicine, University of Rijeka, Rijeka 51000, Croatia; [c]Department of Physics of Complex Systems, Weizmann Institute of Science, Rehovot 76100, Israel; and [d]de Botton Institute for Protein Profiling, The Nancy and Stephen Grand Israel National Center for Personalized Medicine, Weizmann Institute of Science, Rehovot 76100, Israel

Edited by Carol Prives, Columbia University, New York, NY, and approved November 23, 2016 (received for review September 6, 2016)

The microRNA miR-504 targets TP53 mRNA encoding the p53 tumor suppressor. miR-504 resides within the fibroblast growth factor 13 (*FGF13*) gene, which is overexpressed in various cancers. We report that the *FGF13* locus, comprising *FGF13* and miR-504, is transcriptionally repressed by p53, defining an additional negative feedback loop in the p53 network. Furthermore, we show that FGF13 1A is a nucleolar protein that represses ribosomal RNA transcription and attenuates protein synthesis. Importantly, in cancer cells expressing high levels of FGF13, the depletion of FGF13 elicits increased proteostasis stress, associated with the accumulation of reactive oxygen species and apoptosis. Notably, stepwise neoplastic transformation is accompanied by a gradual increase in FGF13 expression and increased dependence on FGF13 for survival ("nononcogene addiction"). Moreover, FGF13 overexpression enables cells to cope more effectively with the stress elicited by oncogenic Ras protein. We propose that, in cells in which activated oncogenes drive excessive protein synthesis, FGF13 may favor survival by maintaining translation rates at a level compatible with the protein quality-control capacity of the cell. Thus, FGF13 may serve as an enabler, allowing cancer cells to evade proteostasis stress triggered by oncogene activation.

proteostasis | p53 | miR-504 | FGF13 | ribosomal biogenesis

MicroRNAs (miRNAs) are endogenous noncoding small RNA molecules (~22 nucleotides) that regulate gene expression, particularly at the posttranscriptional level (1). Interestingly, many miRNAs reside within introns of protein-coding genes and are often derived from a common primary transcript that also gives rise to the mature mRNA of their host gene (2). In such cases, the miRNA biogenesis machinery excises the miRNA precursor (pre-miRNA) from the intron, eventually converting it into the mature miRNA (3).

miR-504 is an intronic miRNA that targets TP53 mRNA encoding the p53 tumor suppressor protein (4). miR-504 reduces p53 mRNA and protein levels and attenuates cellular p53 activity. p53 serves as a major barrier against cancer, acting primarily as a transcription factor that regulates cell-fate decisions, including cell death and cellular senescence, as well as metabolic homeostasis (5–7). As a consequence of its ability to down-regulate p53, miR-504 overexpression hampers p53-mediated responses such as cell-cycle arrest and apoptosis and promotes tumorigenesis (4).

Intriguingly, miR-504 resides within an intron of the fibroblast growth factor 13 (*FGF13*) gene (Fig. S1*A*), a member of the FGF homologous factors (FHF) family. The proteins comprising this family (FGF11, FGF12, FGF13, and FGF14, also called FHF3, FHF1, FHF2, and FHF4, respectively) bear substantial sequence homology to the core region of the canonical FGF superfamily but differ from the other FGF proteins in their inability to activate FGF receptors and thus to function as "real" growth factors (8). Indeed, the FHFs are intracellular proteins that interact with various intracellular partners (9, 10).

FGF13 (FHF2), originally cloned from an ovarian cancer cell line library, is conserved among vertebrates and is normally expressed most abundantly in the brain (10–13). The *FGF13* gene generates a number of transcripts arising through alternative splicing and distinct transcription start sites (14) and differing from each other in their 5′ exons; these isoforms are commonly referred to as "1S" (FGF13 1A), "1U" (FGF13 1B), "1V," "1Y," and "1V+1Y" (Fig. S1*A*). These variants are differentially expressed in tissues and localize to diverse cellular compartments (15), suggesting that they may possess distinct properties and functions. Interestingly, FGF13 is overexpressed in several types of cancer (16, 17).

Intronic miRNAs have roles that may complement (18, 19) or sometimes actually antagonize those of their host genes (20). We now show that expression of the *FGF13* locus, including miR-504, is negatively regulated by p53. Thus, inhibition of miR-504 expression by p53 defines a p53-regulatory negative feedback loop. Importantly, we demonstrate that elevated expression of FGF13 in cancer-derived cells contributes to their survival. We show that the FGF13 1A protein is a nucleolar inhibitor of rRNA synthesis, and its down-regulation in cancer cells induces proteostasis stress, reactive oxygen species (ROS) accumulation, and cell death. Our findings are consistent with the conjecture that oncogenic transformation, which pushes the protein synthesis machinery into excessive activity, induces an increase in misfolded or otherwise

Significance

MicroRNAs (miRNAs) can regulate the amounts of specific proteins by targeting their mRNA. miR-504, which targets the mRNA encoding the p53 tumor suppressor, resides within an intron of the fibroblast growth factor 13 (*FGF13*) gene. We show that expression of the FGF13/miR-504 locus is repressed by p53, defining an additional p53-regulatory feedback loop. Moreover, we report that the FGF13 protein, whose expression is upregulated in a subset of tumors, is essential for survival of cells derived from such tumors. Remarkably, FGF13 restricts the production of ribosomal RNA and attenuates protein synthesis. By tuning down protein synthesis, FGF13 upregulation might enable oncogene-driven cancer cells to avoid excessive accumulation of potentially toxic aberrant proteins, conferring a survival advantage. This work defines a unique vulnerability of cancer cells.

Author contributions: D.R.B., S.V., and M.O. designed research; D.R.B., S.B., I.O., O.T., O.M., G.F., and Y.L. performed research; S.V. contributed new reagents/analytic tools; D.R.B., M.S., T.S., E.K., Y.H., S.V., and M.O. analyzed data; and D.R.B. and M.O. wrote the paper.

The authors declare no conflict of interest.

This article is a PNAS Direct Submission.

See Commentary on page 632.

[1]Present address: Dana-Farber Cancer Institute, Harvard Medical School, Boston, MA 02115.

[2]Present address: Research Center for Digestive Tract and Liver Diseases, Tel Aviv-Sourasky Medical Center, The Sackler Faculty of Medicine, Tel-Aviv University, Ramat-Aviv 69978, Israel.

[3]To whom correspondence should be addressed. Email: moshe.oren@weizmann.ac.il.

This article contains supporting information online at www.pnas.org/lookup/suppl/doi:10.1073/pnas.1614876114/-/DCSupplemental.

aberrant proteins. We propose that by attenuating rRNA synthesis, the up-regulated FGF13 1A mitigates oncogene-associated proteostasis stress and facilitates the survival of transformed cells. Thus, although the augmented FGF13 expression in tumors is unlikely to be a cancer driver, it is not merely a passenger, because it allows the cancer cells to cope with undesirable side effects of oncogene activation. As such, FGF13 may be viewed as a cancer facilitator or "enabler," representing an example of nononcogene addiction whose targeted reversal might render tumors more vulnerable (21).

Results

Expression of the *FGF13*/miR-504 Unit Is Negatively Regulated by p53. To determine whether the in vivo expression pattern of miR-504 correlates with that of its *FGF13* host gene, we analyzed lung cancer data from the Cancer Genome Atlas (TCGA) project (22); indeed, a significant positive correlation was observed (Fig. 1*A*). Hence, FGF13 and miR-504 probably share a common primary transcript [or transcripts; the *FGF13* gene has multiple transcription start sites (Fig. S1*A*), giving rise to multiple primary transcripts]. Notably, FGF13 mRNA is significantly elevated in a subset of lung adenocarcinomas,

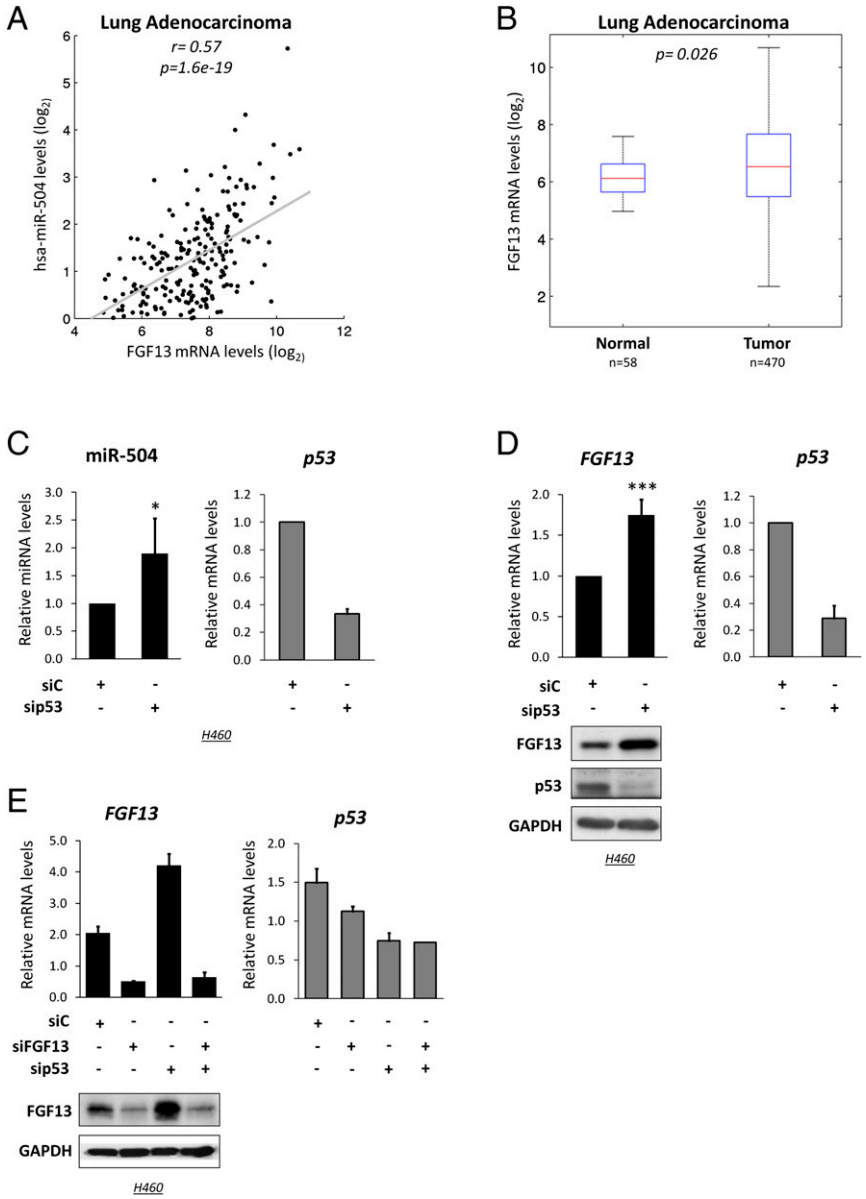

Fig. 1. Expression of the FGF13/miR-504 unit is up-regulated in lung cancer and is negatively regulated by p53. (*A*) Dot plot of *FGF13* mRNA and hsa-miR-504 expression levels in lung adenocarcinoma samples from TCGA. Zero miRNA expression values were ignored. Spearman correlation and *P* values are indicated. (*B*) Box plot of *FGF13* mRNA in normal and tumor samples in the TCGA lung adenocarcinoma dataset. The *P* value was calculated using the rank-sum test. Outliers were eliminated from box plots. *n* = number of samples analyzed. (*C*, *Left*) qPCR analysis of miR-504 expression normalized to small nucleolar RNA, C/D box 44 (SNORD44) in H460 cells after transient transfection with p53 siRNA (sip53) or control siRNA (siC) for 48 h. (*Right*) qPCR analysis of p53 mRNA; values were normalized to GAPDH. Data are expressed as means ± SD from three independent experiments. $*P < 0.05$. (*D*, *Upper*) FGF13 and p53 mRNA expression, normalized to GAPDH, of cells treated as in *C*. Data are expressed as means ± SD from three independent experiments. $***P < 0.001$. (*Lower*) Cell lysates from the same experiment were subjected to Western blot analysis with the indicated antibodies. GAPDH served as loading control. (*E*, *Upper*) FGF13 and p53 mRNA expression, normalized to GAPDH, 48 h after transient transfection of H460 cells with siRNAs targeting p53 (sip53), FGF13 (siFGF13), control siRNA (siC), or combinations thereof. Data are expressed as means ± SD of duplicates from a representative of three independent experiments. (*Lower*) Western blot analysis of the same experiment with antibodies against FGF13 and GAPDH (loading control).

relative to normal lung tissue (Fig. 1*B*). Likewise, a fraction of nonsmall cell lung carcinomas (NSCLC) display *FGF13* amplification and/or overexpression (Fig. S1*B*). Moreover, miR-504 is often up-regulated in EGF receptor-mutant NSCLC (23). These observations suggest that elevated expression of FGF13 and miR-504 may endow a subset of lung tumors with a selective advantage.

To explore the relevance of FGF13 overexpression in lung cancer, we used the human NSCLC cell line H460 expressing abundant FGF13 and miR-504. H460 cells harbor mutant K-Ras protein and retain WT p53. Remarkably, siRNA-mediated p53 silencing increased miR-504 (Fig. 1*C*) and FGF13 mRNA and protein (Fig. 1 *D* and *E*), as also confirmed with a different p53 siRNA (Fig. S1*C*). Quantitative PCR (qPCR) analysis revealed that H460 cells express high levels of the 1A isoform, and this expression is up-regulated upon p53 knockdown (Fig. S1*D*). Thus, p53 restricts the expression of its negative regulator miR-504 and its host gene *FGF13*. The underlying mechanism might be indirect, because we could not detect binding of p53 to the *FGF13* promoter region in ChIP assays, nor is such binding suggested by previously published ChIP-sequencing data.

FGF13 Restricts ROS Accumulation and Promotes Cancer Cell Survival. *FGF13* is overexpressed in a subset of lung cancers (Fig. S1*B*), suggesting that its up-regulation might benefit the cancer cells. Indeed, transient FGF13 knockdown reduced the clonogenicity of H460 cells (Fig. 2*A*). Remarkably, FGF13-silenced cells displayed a substantial increase in the sub-G1 population, detected by flow cytometry (Fig. 2*B*), and in poly(ADP ribose)polymerase (PARP) cleavage (Fig. 2*C*), indicative of apoptosis. A similar effect was observed in another FGF13-high NSCLC cell line, H1437 (Fig. S2*A*). Of note, FGF13 silencing did not affect miR-504 expression significantly (Fig. S2*B*).

Augmented apoptosis also was elicited by siRNA specifically targeting the FGF13 1A isoform (Fig. 2*D*). FGF13 knockdown-induced apoptosis was attenuated by the pan-caspase inhibitor z-VAD-FMK (Fig. S2*C*), confirming that it was at least partially caspase-dependent. In contrast, p53 depletion did not attenuate FGF13 knockdown-induced apoptosis (Fig. S2*D*), implying that p53 is not required for this death. Rather, p53 depletion appeared to augment cell death even further, although the effect did not reach statistical significance (Fig. S2*D*).

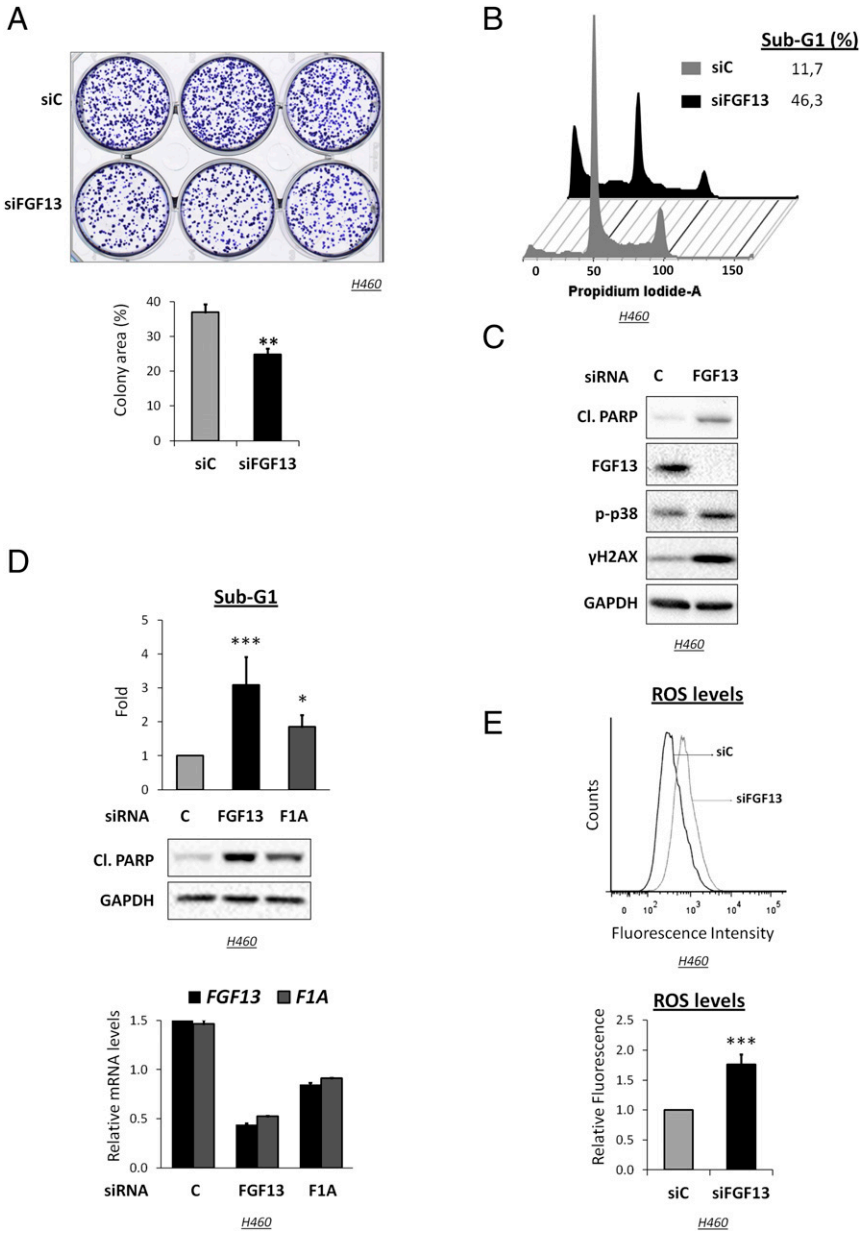

Fig. 2. FGF13 depletion induces apoptosis and up-regulates ROS in H460 cells. (*A*) Representative clonogenic assay of H460 cells transfected with FGF13 siRNA (siFGF13) or control siRNA (siC) for 6 h and then seeded in triplicate at equal cell density in six-well plates. Colonies were stained with crystal violet and scanned (*Upper*) and were quantified (*Lower*) as described in *SI Materials and Methods*. $^{**}P < 0.01$. (*B*) Representative image of FACS-assisted analysis of the DNA content of cells transfected with FGF13 siRNA (siFGF13) or control siRNA (siC) for 48 h. The percentage of cells with sub-G1 DNA content is indicated. (*C*) Western blot analysis with antibodies to the indicated proteins 48 h after transient transfection of H460 cells with FGF13 (FGF13) or control (C) siRNA. Cl. PARP, cleaved PARP. GAPDH served as loading control. (*D*, *Top*) Percentage of cells with sub-G1 DNA content based on FACS analysis of H460 cells transiently transfected for 48 h with FGF13 siRNA (FGF13), control siRNA (C), or siRNA specific for the FGF13 1A isoform (F1A). Data are expressed as fold change and represent the means ± SD from three independent experiments. $^{***}P < 0.001$, $^{*}P < 0.05$ versus control siRNA. (*Middle*) Lysates of cells transfected as above were subjected to Western blot analysis with the indicated antibodies. (*Bottom*) qPCR analysis of FGF13 mRNA normalized to GAPDH to monitor FGF13 knockdown in the above experiment. qPCR was performed with primers specific for the 1A isoform (F1A) or common to all isoforms (FGF13). (*E*, *Upper*) Cells treated as in *C* were stained with the fluorescent dye H2DCFDA to measure ROS levels by FACS analysis. (*Lower*) Relative H2DCFDA fluorescence; data are expressed as the means ± SD from three independent experiments. $^{***}P < 0.001$.

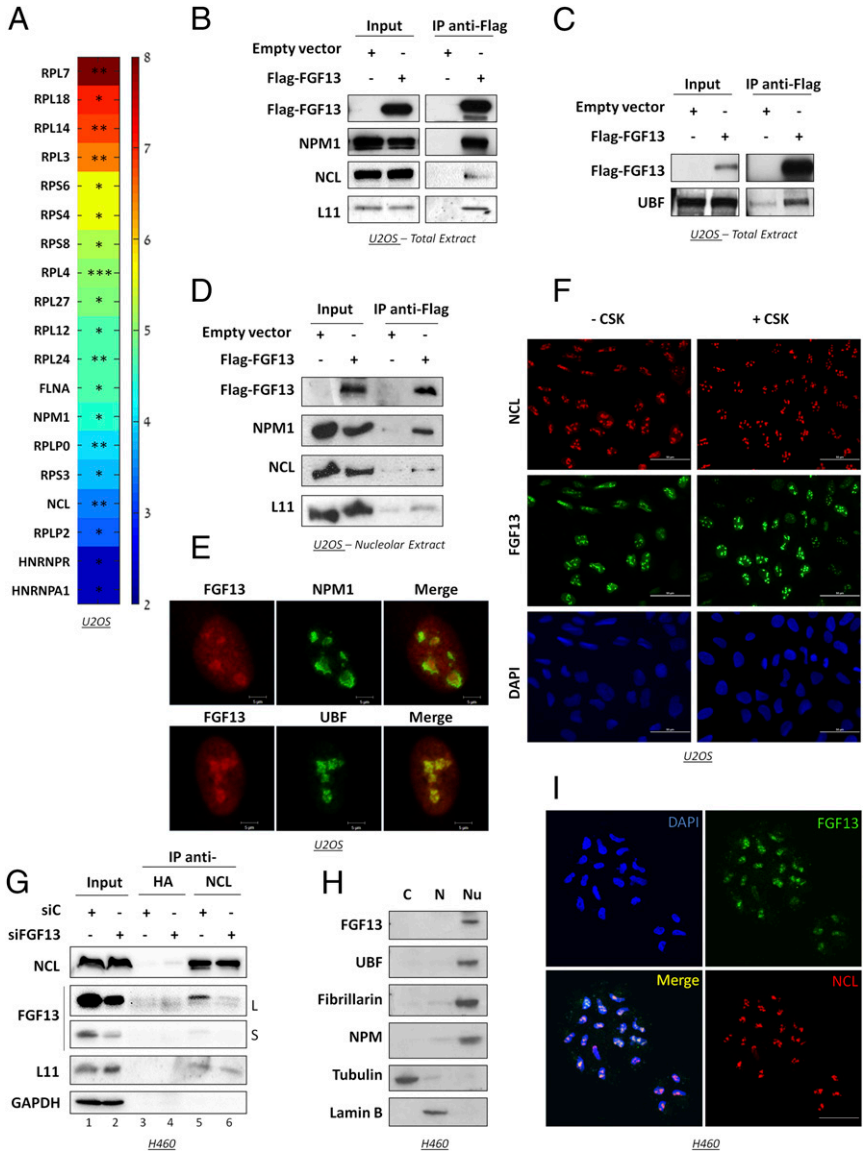

Fig. 3. Binding partners and nucleolar localization of FGF13. (*A*) Heat map of the spectral counts of FGF13-interacting proteins identified by mass spectrometry in U2OS cells stably expressing Flag-FGF13 1A. See *SI Materials and Methods*. ***$P < 0.001$, **$P < 0.01$, *$P < 0.05$ versus U2OS cells stably transfected with empty vector. (*B*) U2OS cells stably expressing Flag-FGF13 1A or empty vector were subjected to IP with anti-Flag antibodies followed by Western blot analysis with antibodies specific for Flag, B23/nucleophosmin (NPM1), NCL, or RPL11 (L11). (*C*) Cells were subjected to IP as in *B*, except that bound proteins were eluted from the anti-Flag beads with excess Flag epitope peptide and then were subjected to Western blot analysis with antibodies specific for Flag or UBF. (*D*) Nucleoli were isolated from U2OS cells stably expressing Flag-FGF13 1A or empty vector. Nucleolar extracts were subjected to IP with anti-Flag antibodies, followed by Western blot analysis with the indicated antibodies. (*E*) U2OS cells stably expressing Flag-FGF13 1A were subjected to immunofluorescence staining with anti-Flag (to visualize FGF13 1A) (*Left*) or anti-B23/nucleophosmin (NPM1) (*Upper Center*), or anti-UBF (*Lower Center*) antibodies. (*Right*) Merged images in which yellow represents regions of colocalization. (Scale bars, 5 μm.) (*F*) As in *E*, cells were either treated (+) or not treated (–) with CSK buffer (*SI Materials and Methods*) and were stained with antibodies against Flag or nucleolin (NCL). Nuclear DNA was stained with DAPI (blue). (Scale bars, 50 μm.) (*G*) H460 cells were transfected with FGF13 siRNA (siFGF13) or control siRNA (siC). Forty-eight hours later, cells were subjected to IP with an antibody against nucleolin (NCL) or anti-HA as control, followed by Western blot analysis with the indicated antibodies. RPL11 (L11), a known NCL interactor, served as positive control. GAPDH served as loading control. Short (S) and long (L) exposures of FGF13 are shown. (*H*) H460 cells were fractionated into cytosolic (C), nuclear (N), and nucleolar (Nu) fractions, followed by Western blot analysis with the indicated antibodies. Tubulin, lamin B, and fibrillarin served as markers for the cytosolic, nuclear, and nucleolar fractions, respectively. (*I*) H460 cells were extracted with CSK buffer as in *F* and were subjected to immunofluorescence staining with antibodies against FGF13 (green) (*Upper Right*) or nucleolin (NCL, red) (*Lower Right*) along with DAPI (blue) (*Upper Left*) for DNA. (*Lower Left*) A merged image of all three stains. (Scale bar, 50 μm.)

Additionally, phosphorylated p38 and phosphorylated histone 2A variant H2AX (γ-H2AX) were elevated (Fig. 2*C*), indicative of stress and DNA damage, respectively.

Notably, FGF13 silencing increased cellular ROS (Fig. 2*E*) 24 h after siRNA transfection (Fig. S2*E*). The free radical scavenger *N*-acetylcysteine (NAC) provided a modest but significant rescue from apoptosis (Fig. S2*F*), suggesting that increased ROS is partly responsible for cell death upon FGF13 down-regulation. Remarkably, comparable ROS up-regulation also was elicited by p53 silencing (Fig. S2*G*). Hence, both FGF13 and p53 restrict ROS production in these cells.

Overall, these findings suggest that elevated FGF13 supports homeostasis in lung cancer cells, mitigating oxidative stress and promoting survival.

FGF13 1A Is a Nucleolar Protein. Although FGF13 1B binding partners have been described (24, 25), the FGF13 1A interactome remained unexplored. Therefore, U2OS cells expressing low levels of FGF13 were stably transduced with Flag-FGF13 1A, which then was immunoprecipitated and subjected to mass spectrometry analysis to identify putative interactors. Interestingly, these were highly enriched for nucleolar proteins, including nucleolin, B23/nucleophosmin (NPM1), and numerous ribosomal proteins (Fig. 3*A*), suggesting, in agreement with an earlier report (15), that FGF13 1A resides mainly in the nucleolus. Coimmunoprecipitation analysis confirmed the association of Flag-FGF13 1A with several endogenous nucleolar proteins, including ribosomal protein L11 (RPL11) (Fig. 3*B*) and the transcription factor upstream binding factor (UBF) (Fig. 3*C*), a positive regulator of rRNA synthesis. Subcellular fractionation confirmed binding of Flag-FGF13 to NPM1, nucleolin, and RPL11 in the nucleolar fraction, demonstrated by immunoprecipitation (IP) with Flag (Fig. 3*D*), NPM1 (Fig. S3*A*), or nucleolin (Fig. S3*B*) antibodies.

Indeed, immunofluorescence staining revealed predominantly nucleolar Flag-FGF13 1A localization (Fig. 3*E*), with a weak nucleoplasmic signal. Flag-FGF13 1A colocalized closely with UBF in the fibrillar center and the dense fibrillar component (Fig. 3*E*, *Lower*); partial overlap with NPM1 in the granular component was observed also (Fig. 3*E*, *Upper*).

Prediction of nucleolar localization sequences (NoLS) (26, 27) suggested that FGF13 1A contains such elements near its N terminus (Fig. S3*C*), a region absent in FGF13 isoforms reported to be cytoplasmic (15). Furthermore, upon actinomycin D-mediated inhibition of rRNA synthesis, FGF13 1A redistributed to the nucleoplasm (Fig. S3*D*), like other nucleolar proteins (28). Notably, removal of soluble cytoplasmic and nuclear proteins through detergent extraction [CytoSKeleton (CSK)] before fixation confirmed the tight nucleolar association of Flag-FGF13, similar to that of nucleolin (Fig. 3*F*). IP analysis validated a specific interaction of endogenous FGF13 with nucleolin (Fig. 3*G*, compare lane 3 with lane 5), and cell fractionation corroborated its nucleolar distribution (Fig. 3*H*). Importantly, endogenous FGF13 remained associated with the nucleolar compartment after detergent extraction (Fig. 3*I*). Thus, FGF13 1A is a bona fide nucleolar protein.

FGF13 Depletion Augments Nucleolar Size and Increases rRNA and Protein Synthesis. FGF13 silencing led to a significant increase in average nucleolar size, revealed by fibrillarin, UBF, and NPM1 staining (Fig. 4 *A* and *B*; quantification in Fig. 4 *C* and *D*). The total number of nucleoli per cell was unaffected (Fig. S3*E*).

The nucleolus is the site of ribosomal biogenesis, including transcription and processing of rRNA. Nucleolar enlargement is often associated with increased rRNA content (29). We therefore assessed the impact of FGF13 down-regulation on rRNA synthesis by quantifying 47S precursor rRNA (pre-rRNA). Remarkably, FGF13 knockdown strongly up-regulated 47S pre-rRNA (Fig. 4*E*). The effect was most prominent 24 h after transfection and was attenuated at 48 h (Fig. 4*F*), probably reflecting adaptation through a negative feedback loop or merely that the cells were gradually undergoing stress-induced apoptosis. In either case, these results imply that elevated FGF13 restricts rRNA synthesis in these cancer cells.

Augmented rRNA production is usually coupled with increased protein synthesis. Therefore we assessed protein synthesis rates, using the puromycin analog O-propargyl-puromycin (OPP), which is incorporated into newly translated polypeptides and can be fluorescently labeled. Indeed, FGF13 depletion augmented protein synthesis (Fig. 5 *A* and *C*), and this augmented synthesis was abolished by the protein synthesis inhibitor cycloheximide (CHX). Quantification of fluorescence intensity by microscopy (Fig. 5*B*) and by FACS (Fig. 5*D*) confirmed the increase in newly translated polypeptides. Notably, the effect was more modest than the corresponding increase in rRNA synthesis. FGF13-depleted cells also displayed enhanced mTOR activity, evident by increased phosphorylation of S6 kinase, RPS6, and 4EBP1 (Fig. 5*E*).

Next, we performed RNA sequencing (RNA-seq) analysis on H460 cells without and with FGF13 knockdown (Table S1). Gene Ontology (GO) enrichment analysis (Table S2) revealed that FGF13 depletion induced processes associated with disrupted protein homeostasis (proteostasis), including the unfolded protein response (UPR) and the heat-shock response (HSR) (Fig. 5*F*). Concomitantly, FGF13 depletion led to the accumulation of CCAAT-enhancer–binding protein homologous protein (CHOP) and spliced x-box binding protein-1 (sXBP1) mRNA (Fig. S4), indicative of an endoplasmic reticulum (ER) stress response.

Exposure to the proteasome inhibitor MG132 augments the accumulation of aberrant proteins and activates the HSR (30). We reasoned that combining MG132 with FGF13 knockdown might further exacerbate proteostasis stress. Indeed, combined treatment resulted in augmented HSR, exemplified by up-regulation of heat-shock protein A6 (HSPA6) mRNA (Fig. 5*G*) encoding the heat-shock 70-kD protein (HSP70) family member HSP70B′, which localizes to the nucleolus upon heat shock (31).

Together, these observations imply that elevated FGF13 can protect cancer cells against proteostasis stress, probably by tuning down protein synthesis and thereby avoiding excessive emergence of aberrant polypeptides.

FGF13 Is Up-Regulated During Neoplastic Transformation to Promote Transformed Cell Survival. To explore further links between FGF13 up-regulation and cancer, we used an in vitro progression series comprising slow-growing telomerase-immortalized WI-38 human lung embryonic fibroblasts (WI-38^{Slow}), their fast-growing derivatives obtained through extended passaging in culture (WI-38^{Fast}) (32, 33), and WI-38^{Fast} cells transduced with activated mutant H-Ras^{V12} and selected for escape from p53-mediated antiproliferative checkpoints, giving rise to stably transformed cells (escapers, WI-38^{Ras}) (34).

Remarkably, although FGF13 expression was almost undetectable in parental WI-38^{Slow} cells, it became up-regulated in WI-38^{Fast} cells and further increased greatly in the WI-38^{Ras} escapers (Fig. 6*A*). miR-504 followed the same trend (Fig. 6*B*), suggesting positive selection for elevated expression of the *FGF13* locus during transformation. In further support of selection, rather than direct up-regulation, transient overexpression of H-Ras^{V12} in WI-38^{Fast} cells did not increase FGF13 mRNA (Fig. S5*A*). Actually, oncogenic Ras was reported to repress FGF13 expression in other cells (35). To investigate the dynamics of this process, WI-38^{Fast} cells were transduced with H-Ras^{V12}. As seen in Fig. S5*B*, FGF13 mRNA started rising only ∼10 d after H-Ras^{V12} transduction. The gradual increase in FGF13 mRNA might be facilitated by epigenetic attenuation of p53 activity during establishment of the escaper population (34).

WI-38^{Ras} cells display elevated ROS, relative to their WI-38^{Fast} progenitors (Fig. 6*C*), probably because of constitutive Ras activation (36). FGF13 1A knockdown elicited a very slight increase in ROS in WI-38^{Fast} but a significant increase in WI-38^{Ras} cells (Fig. 6*D*). Concomitantly, FGF13 1A-silenced WI-38^{Ras} cells displayed elevated phospho-p38 and cleaved PARP and a marked increase in the sub-G1 subpopulation (Fig. 6*E*), indicative of exacerbated stress-induced apoptosis. Of note, silencing all FGF13 isoforms together did not exert a stronger effect than silencing FGF13 1A alone (Fig. S5 *C* and *D*). As expected, FGF13 siRNA did not affect the viability of WI-38^{slow} cells (Fig. S5*E*), which hardly express FGF13 mRNA. In agreement with its effects on ROS and apoptosis, FGF13 1A depletion reduced the clonogenicity of WI-38^{Ras} cells more than that of WI-38^{Fast} cells (Fig. 6 *F* and *G*). Thus, WI-38 cells accrue a gradual increase in FGF13 expression as they progress along the transformation axis and become increasingly "addicted" to FGF13 overexpression as a survival mechanism.

To address the impact of FGF13 up-regulation during Ras-induced transformation more directly, WI-38^{Fast} cells were transduced with H-Ras^{V12}, either alone or in combination with FGF13 1A. Acute H-Ras^{V12} overexpression led to a substantial reduction in cell number (Fig. 6*H*, *Upper*), in association with increased cell death as assessed by propidium iodide uptake (Fig. S5*F*). Notably, WI-38^{Fast} cells have silenced p16 and p14^{ARF} expression (32) and tend to undergo apoptosis, rather than senescence, upon Ras hyperactivation (34).

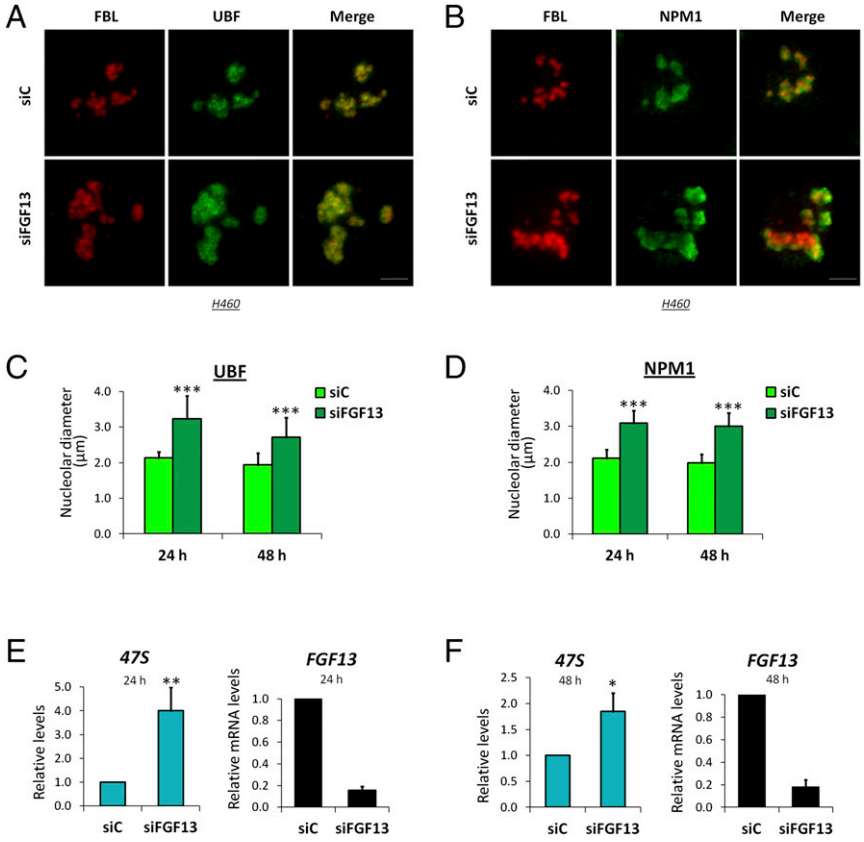

Fig. 4. FGF13 depletion augments nucleolar size and increases ribosomal RNA synthesis. (*A* and *B*) H460 cells were transiently transfected with FGF13 siRNA (siFGF13) or control siRNA (siC) and 24 h later were subjected to immunofluorescence staining with antibodies against the nucleolar proteins fibrillarin (FBL, red), UBF (green) (*A*), and B23/nucleophosmin (NPM1) (green) (*B*). (Scale bar, 5 μm.) (*C* and *D*) Quantification of nucleolar diameter performed on cells stained with an anti-UBF (*C*) or anti-NPM1 (*D*) antibody 24 or 48 h after transfection as in *A* and *B* (*SI Materials and Methods*). Data are shown as means ± SD from 15 cells per condition, from two independent experiments. ***$P < 0.001$. (*E* and *F*) H460 cells were transfected as in *A* and *B*, and RNA was extracted 24 (*E*) or 48 (*F*) h after transfection and subjected to qPCR analysis of *47S* pre-rRNA and FGF13 mRNA, normalized to GAPDH. Data are expressed as mean ± SD from three independent experiments. **$P < 0.01$, *$P < 0.05$.

Concomitantly, Ras^{V12} decreased the clonogenic survival of $WI\text{-}38^{Fast}$ cells (Fig. 6*H*). Thus, FGF13 1A overexpression reduced $H\text{-}Ras^{V12}$–induced cell death, mitigated the decrease in cell number, restored the clonogenic capacity of $H\text{-}Ras^{V12}$–infected cells, and enabled the retention of higher mutant Ras expression (Fig. S5*G*).

Hence, although FGF13 1A expression is not directly modulated by activated Ras, it is gradually up-regulated during stabilization of the transformation process, enabling mutant Ras-expressing cells to cope better with oncogene-induced stress.

Discussion

miR-504 is a negative regulator of p53, directly targeting p53 mRNA and quenching p53 levels and activity (4). In agreement with a putative oncogenic role, miR-504 is overexpressed in a variety of cancers (4, 37–40). However, relatively little is known about the mechanisms that control miR-504 expression, beyond its down-regulation by the secreted factors CTGF and TFF1 (38, 39). We now show that miR-504, along with its host gene *FGF13*, is subject to constitutive transcriptional repression by p53. This finding is consistent with an earlier study, in which MMTV–Wnt–induced mouse mammary tumors emerging on a $p53^{+/-}$ background were observed to produce more miR-504 than tumors developing in $p53^{+/+}$ mice (41). The p53–miR-504 negative feedback loop adds a module to the p53 network, possibly acting to boost p53 protein levels further in response to p53-activating signals.

Notably, FGF13-mediated regulation of cell survival does not require WT p53, as observed in H1437 cells harboring mutant p53 (R267P) or upon p53 down-regulation in WT p53 H460 cells. This observation is particularly relevant given the high prevalence of *TP53* mutations in NSCLC (42).

Our study reveals an additional important activity of FGF13. We show that FGF13 1A resides primarily in the cell nucleolus, where it represses rRNA synthesis. Notably, FGF13 1A interacts with UBF, a key mediator of rRNA transcription, suggesting that FGF13 1A may directly inhibit UBF and thereby compromise the ability of RNA polymerase I (Pol I) to transcribe the rDNA genes. In addition, FGF13 may affect RNA Pol I activity by binding nucleolin, whose interaction with RNA Pol I is required for RNA Pol I-mediated transcription (43). Although our study highlights the impact of FGF13 1A, possible contributions of other FGF13 isoforms should not be disregarded. Indeed, some FGF13 isoforms have been associated with cisplatinum resistance (44). Moreover, in neurons, FGF13 1B regulates microtubule dynamics and facilitates cell migration (24). Hence, the loss of p53 function also may promote cancer by up-regulating other FGF13 isoforms.

FGF13 is overexpressed in several types of cancer, including pancreatic endocrine carcinoma (17), melanoma (16), multiple myeloma (45), and lung cancer (this study). FGF13 overexpression might have suggested that FGF13 plays an oncogenic role, a notion seemingly consistent with the repression of its expression by p53. However, we demonstrate here that FGF13 inhibits rRNA and global protein synthesis, as reported for canonical tumor suppressors such as p53 and Arf (46, 47). Conversely, many oncogenes promote ribosomal biogenesis and protein synthesis to facilitate cell growth and proliferation.

So how does one rationalize FGF13 overexpression in cancer? Our study implies that FGF13 up-regulation is not required to drive

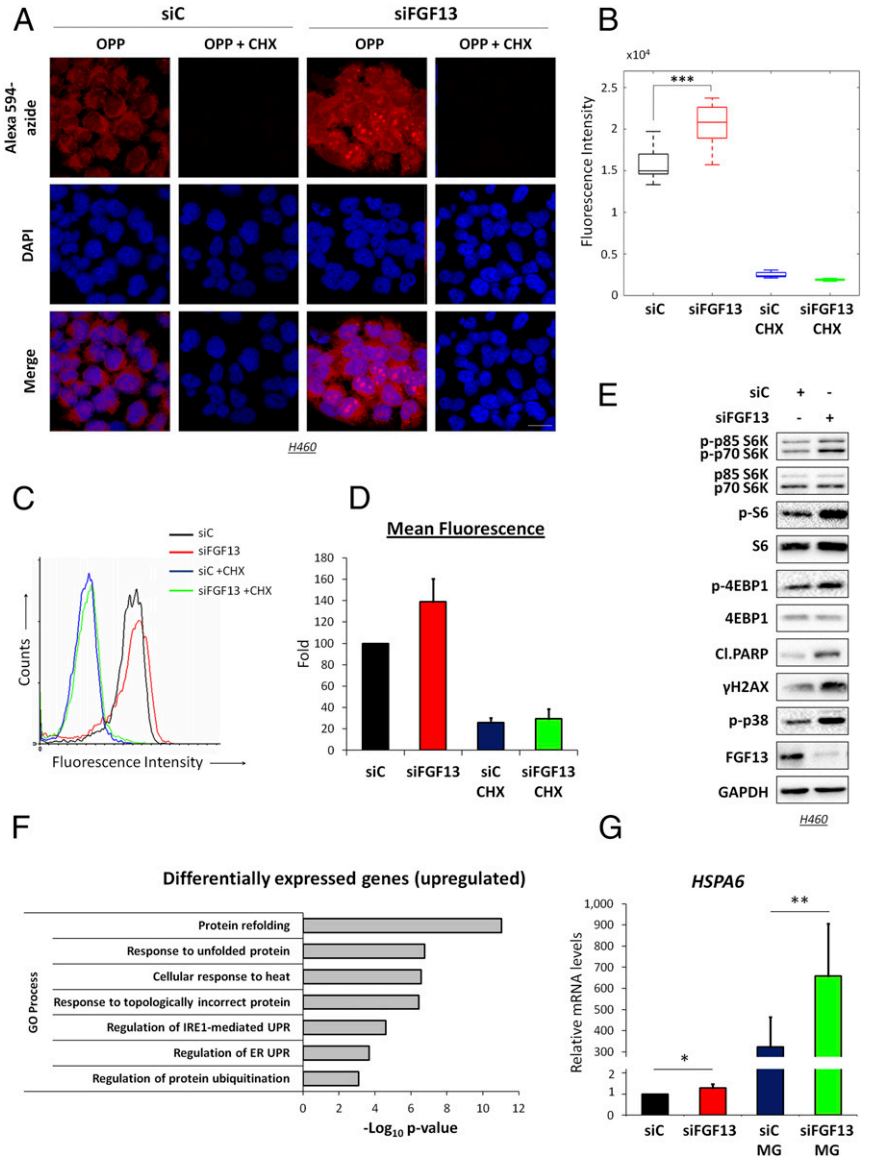

Fig. 5. FGF13 down-regulation augments protein synthesis and induces unfolded protein stress. (*A*) Fluorescence microscopy imaging of protein synthesis in H460 cells transiently transfected with control siRNA (siC) or FGF13 siRNA (siFGF13) for 36 h. Fluorescence staining of nascent polypeptides was done with OPP using Alexa 568-azide (red) along with DAPI (blue) as described in *SI Materials and Methods*. Where indicated, CHX (100 μg/mL) was added to block protein synthesis. (Scale bar, 20 μm.) (*B*) Box plot quantification of Alexa Fluor 568 fluorescence intensity based on 8–10 fields containing ∼1,500 cells per condition, derived from two biological replicates. ***$P < 0.001$. (*C*) Representative FACS analysis of Alexa Fluor 568-azide fluorescence performed on cells treated as in *A*. (*D*) Quantification of FACS analysis done as in *C*. Data are expressed as fold change in Alexa Fluor 568 mean fluorescence intensity ± SD from two independent experiments. (*E*) Western blot analysis with antibodies to the indicated proteins 48 h after transient transfection of H460 cells with FGF13 siRNA (siFGF13) or control siRNA (siC). GAPDH served as loading control. (*F*) GO enrichment analysis of RNA-seq data performed on H460 cells transiently transfected with FGF13 or control siRNAs. GO terms belonging to biological processes were sorted by *P* values. (*G*) RNA was isolated from cells transfected as in *E* and treated or not with 50 μM MG132 (MG) for 4 h. HSPA6 mRNA was quantified by qPCR and normalized to GAPDH. Data are shown as the mean ± SD of three independent experiments. **$P < 0.01$, *$P < 0.05$.

cancer but rather helps the emerging cancer cells to cope with the unwelcome consequences of oncogene activation. Specifically, many oncogenes, as exemplified by c-Myc, BRAF, and Ras, elicit a substantial increase in the rate of protein synthesis; although facilitating cell proliferation, this increased synthesis also overburdens the cellular protein quality control mechanisms, eventually giving rise to ER stress and proteotoxic stress (48–50). Furthermore, mutations in protein-coding regions, frequent in cancer, also increase the load of aberrant proteins and the risk of proteotoxic stress; in that regard, it is remarkable that FGF13 overexpression is observed in lung cancer and melanoma, two cancer types harboring extensive somatic mutations. The challenge to proteostasis in tumor cells may be exacerbated further by the presence of DNA duplications, deletions, and copy number variations, causing imbalance in the stoichiometry of multisubunit complexes (51). We propose that FGF13 up-regulation dampens this proteostasis stress by tuning down the rate of protein synthesis, eventually bringing it to a level that represents a compromise between the need to produce more proteins and the ability of the cancer cell to evade lethal proteotoxic stress. Indeed, translational attenuation can improve translation fidelity, allowing proper folding of newly synthesized peptides and reducing the load on the protein quality control machinery (52).

Furthermore, perturbed proteostasis produces ROS that eventually might trigger apoptosis (53). By moderating the

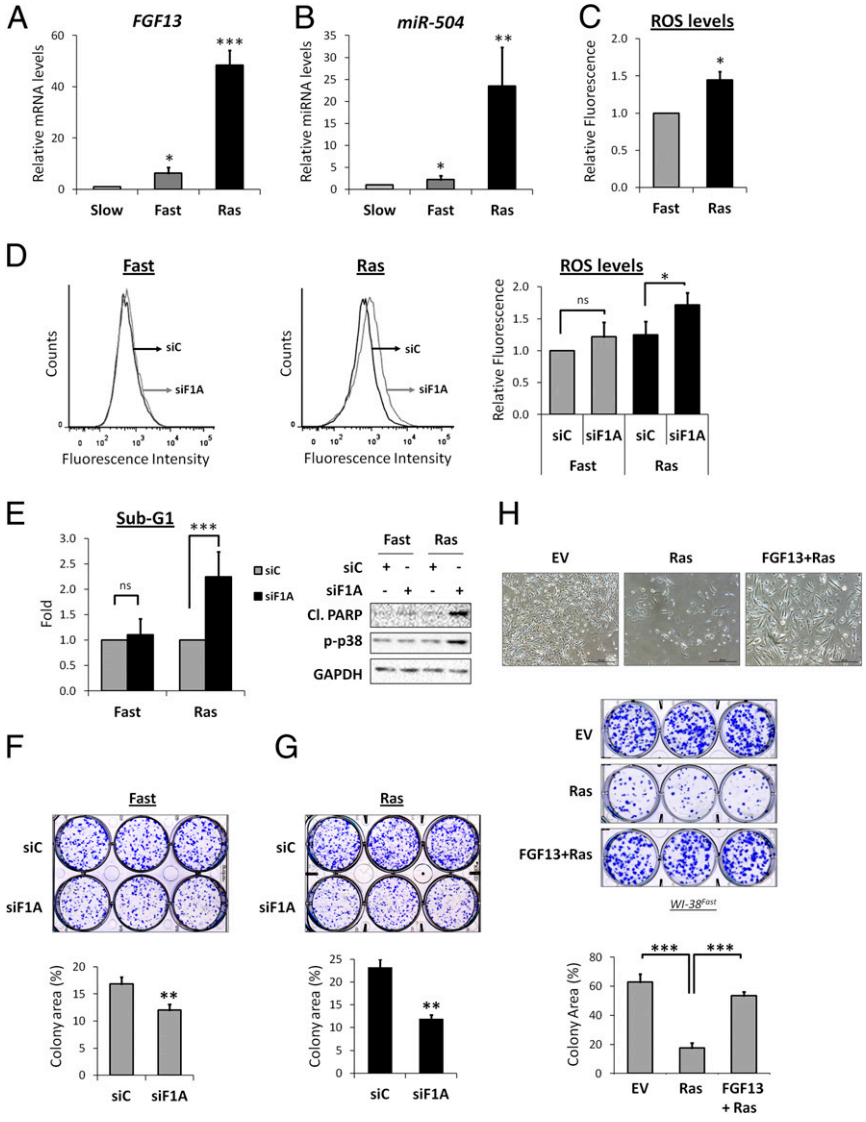

Fig. 6. FGF13 is up-regulated in an in vitro model of cellular transformation and supports the survival of cells overexpressing oncogenic Ras. (*A* and *B*) Cells from a tissue-culture model of neoplastic transformation, comprising immortalized slow-growing WI-38 fibroblasts (WI-38^{Slow}), their rapidly growing derivatives (WI-38^{Fast}), and WI-38^{Fast} cells transformed with a retrovirus encoding mutant H-Ras and selected for escape from Ras-induced antiproliferative checkpoints (WI-38^{Ras}), were subjected to qPCR quantification of *FGF13* mRNA (*A*) or *miR-504* (*B*). Values were normalized to GAPDH or SNORD44, respectively $*P < 0.05$, $**P < 0.01$, $***P < 0.001$. (*C*) WI-38^{Fast} and WI-38^{Ras} cells were stained with H2DCFDA, and ROS levels were determined by FACS. Fluorescence intensity is expressed as fold change. Data are shown as mean ± SD from three independent experiments. $*P < 0.05$. (*D*, *Left* and *Center*) Representative FACS images of WI-38^{Fast} (*Left*) and WI-38^{Ras} (*Center*) cells transiently transfected with FGF13 1A-specific siRNA (siF1A) or control siRNA (siC) for 48 h and stained for ROS as in *C*. (*Right*) Quantification of H2DCFDA fluorescence intensity expressed as fold change. Data are expressed as mean ± SD from three independent experiments. $*P < 0.05$; ns, not significant. (*E*, *Left*) Quantification of the relative proportion of cells with sub-G1 DNA content, deduced from FACS analysis of WI-38^{Fast} and WI-38^{Ras} 72 h after transfection with FGF13 1A-specific siRNA (siF1A) or control siRNA (siC). Data are expressed as fold change of FGF13 1A-specific siRNA relative to the control siRNA of each population. (*Right*) Western blot analysis of representative lysates probed with the indicated antibodies. GAPDH served as loading control. $***P < 0.001$; ns, not significant. (*F* and *G*, *Upper*) Representative images of WI-38^{Fast} (*F*) and WI-38^{Ras} (*G*) cells transfected with FGF13 1A-specific siRNA (siF1A) or control siRNA (siC) for 6 h and subjected to clonogenic assay as in Fig. 2*A*. (*Lower*) Quantification results in upper panels. $**P < 0.01$. (*H*, *Top*) Representative images of WI-38^{Fast} cells infected with empty vector retrovirus (EV) or a retrovirus expressing H-Ras^{V12} (Ras), either alone or together with a retrovirus expressing FGF13 1A (FGF13+Ras). Hygromycin selection was initiated 2 d after infection and was continued for 8 d. Cultures were photographed 14 d after infection through a 4× phase-contrast objective. (Scale bars, 500 μm.) (*Middle*) Representative picture of a clonogenic assay of WI-38^{Fast} cells infected as described above. After 8 d of drug selection cells were seeded in triplicate at an equal cell density in six-well plates and were maintained without drug for an additional 11 d. (*Bottom*) Colonies then were stained with crystal violet, scanned, and quantified as described in *SI Materials and Methods*. $***P < 0.001$.

increase in protein synthesis and quenching ROS accumulation, FGF13 might support cancer cell survival without compromising the other cancer-promoting effects of activated oncogenes. Of note, FGF13 is also overexpressed in cell lines derived from multiple myeloma (45), a malignancy characterized by persistent proteostasis stress and highly reliant on mechanisms that cope with such stress (54).

It is also conceivable that different components of the protein synthesis machinery, whose levels are tightly coordinated in normal cells, become differentially deregulated upon oncogenic activation, creating a chronic imbalance. Of note, excessive accumulation of nascent rRNA can directly cause DNA damage by forming rRNA:rDNA hybrids (55). Thus, the incipient cancer cell may remedy an imbalance between different components of the protein

biosynthetic machinery by selectively tuning down the component that is most aberrantly up-regulated. We propose that when that component is rRNA transcription, remedy can be achieved by increasing FGF13, thereby putting an adjustable brake on rRNA synthesis. This effect is reminiscent of RUNX1 mutations in myelodysplastic syndrome, which reduce rRNA synthesis and ribosomal biogenesis, tune down p53 levels, and render hematopoietic stem cells more resilient to stress-induced apoptosis (56). Interestingly, the PHF6 protein, which, like FGF13, interacts with UBF and represses rRNA synthesis (55), is overexpressed in B-cell lymphoma and has been suggested to play a role in progression of this malignancy (57), often driven by c-Myc hyperactivation.

As shown here, stepwise transformation is accompanied by progressive up-regulation of FGF13, along with increased dependence on FGF13 for buffering excessive ROS and for survival. Introduction of oncogenic Ras into WI-38^{Fast} cells triggers extensive apoptosis and senescence; only a minor fraction of the cells escape these failsafe checkpoints, eventually giving rise to stably transformed progeny (34). Our data suggest that FGF13 up-regulation is selected for during this stabilization period, because it enables the cancer cells to cope more effectively with the chronic proteostasis stress imposed by Ras activation. In the course of this process, the transformed cells might become addicted to high levels of FGF13, as indicated by their propensity to undergo apoptosis upon FGF13 depletion.

In nontransformed cells, negative regulation of FGF13 by p53 may serve to ensure the robustness of protein homeostasis. Transient attenuation of p53 activity, which may be desirable under particular physiological conditions (e.g., early embryonic development, wound healing), might endanger the cell by allowing excessive ROS accumulation (58) (see also Fig. S2*E*). Concurrent transient up-regulation of FGF13 resulting from attenuated p53 activity may help avert these undesirable consequences by providing an alternative layer of protection. This concerted action is made even more effective by the simultaneous up-regulation of miR-504, which reinforces the quenching of p53 activity. Importantly, we surmise that in normal cells this circuit is dynamically regulated, temporally and spatially, assuring its transient nature. However, cancer cells that retain WT p53 might co-opt this mechanism and fix it in an "on" state, thereby blunting p53 by the excessive miR-504 and simultaneously gaining FGF13-mediated protection against potential proteostasis stress imposed by oncogenic events. Such cells will be more likely to possess a long-term competitive advantage.

In sum, although FGF13 is highly unlikely to play a role in driving cancer, our findings suggest that it nevertheless is a facilitator of cancer progression. In fact, FGF13 may be viewed as an enabler, enabling the emerging tumor cells to cope with the stressful impact of cancer-associated deregulation of key cellular processes. Such enablers allow the cancer cell to reset its metabolic balance and achieve higher biosynthetic rates without going overboard. Concomitantly, these cells acquire an addiction to the enabler, as shown for other buffering proteins such as molecular chaperones (21, 59), thus positioning such enablers as potential targets for cancer therapy.

Materials and Methods

Cell Culture and Chemicals. All cell lines used in this study were grown and maintained as described in *SI Materials and Methods*.

Transfections and Infections. siRNA transfections were performed with Dharmafect 1 reagent (Dharmacon) according to the manufacturer's protocol. siRNAs for FGF13 and p53 were purchased as SMARTpools, and FGF13 1A was purchased as a single oligo (GGCAAGACCAGCUGCGACAUU) from Dharmacon. All siRNA oligos were used at a final concentration of 20 nM except for double-knockdown assays in which 10 nM of each siRNA was used.

Retroviral infection of WI-38^{Fast} cells was performed as previously described (34). Hygromycin selection was initiated 48 h after infection.

Flow Cytometry. Cell-cycle analysis and measurement of endogenous cellular ROS were performed with propidium iodide staining or with the ROS-sensitive dye 2′,7′-dichlorodihydrofluorescein diacetate (H2DCFDA) (Molecular Probes), respectively, as described in *SI Materials and Methods*.

Clonogenic Assay. Six hours after transfection with siRNAs, cells were trypsinized and reseeded in six-well plates at a density of 3,000 cells per well and then were grown until colonies were visible. For infections, 8 days after drug selection the cells were trypsinized and reseeded in six-well plates at a density of 5,000 cells per well. Staining of colonies and analysis are described in *SI Materials and Methods*.

IP. For Flag-FGF13 IP, U2OS cells were harvested, washed with ice-cold PBS, and lysed on ice in NET lysis buffer [50 mM Tris·HCl (pH 7.4), 150 mM NaCl, 1 mM EDTA 0.1% Nonidet P-40] supplemented with protease inhibitor mix (Sigma) and phosphatase inhibitor mixture II and III (Sigma). Cells were sonicated in a Bioruptor sonicator (Diagenode), 30 s on and 60 s off for a total of 10 min, and then were centrifuged at 14,000 × *g* for 10 min at 4 °C. After preclearing, lysates were incubated at 4 °C for 2–4 h with anti-Flag antibodies covalently attached to beads (Sigma). A 1/20 aliquot of the cleared suspension was taken as input. Next, the beads were washed three times with NET buffer, and elution was carried out using a Flag peptide (Sigma) in PBS when indicated. Samples were resolved by SDS/PAGE followed by Western blotting. Nucleolin IP was performed with anti-nucleolin antibody (Abcam) plus protein A-Sepharose beads (Repligen).

Western Blot Analysis. Immunoblot analysis was performed as previously described (60). The list of antibodies used is provided in *SI Materials and Methods*.

Isolation of Total RNA and qPCR. RNA isolation, RT-PCR and qPCR analysis are described in *SI Materials and Methods*. Primer sequences are detailed in *SI Materials and Methods*.

Immunofluorescence Staining. Nucleolar proteins were visualized as previously reported (61) and described in *SI Materials and Methods*.

Cell Fractionation. Cytoplasm, nuclei, and nucleoli were prepared from 10 × 10^6 H460 cells essentially as previously reported (62) and as described in *SI Materials and Methods*.

Measurement of Nucleolar Diameter. The average diameter of the nucleolus was measured in H460 cells stained by indirect immunofluorescence with antibodies against nucleolar proteins UBF or NPM1 using Zeiss LSM700 confocal laser scanning microscopy and analyzed with ZEN imaging software (Carl Zeiss).

Measurement of Protein Synthesis. Newly translated polypeptides were analyzed by using the puromycin analog OPP (Jena Bioscience) with further fluorescent labeling and were quantified by microscopy and by FACS as described in *SI Materials and Methods*.

Database Analysis. Lung adenocarcinoma data were generated by the TCGA Research Network (https://cancergenome.nih.gov/) and were downloaded from TCGA data portal. Outliers were eliminated from box plots.

Mass Spectrometry Analysis. The detailed procedure of sample preparation and a description of data processing, searching, and analysis are provided in *SI Materials and Methods*.

RNA-Seq. Library construction, sequencing, and GO enrichment analysis are described in *SI Materials and Methods*.

Statistical Analysis. Statistical significance was determined using a two-tailed Student's *t* test. Unless stated otherwise, the *P* value was calculated based on three biological replicates.

ACKNOWLEDGMENTS. We thank Lior Golomb for help with confocal microscopy, Varda Rotter for the WI-38 transformation series, and Eytan Domany for fruitful discussions. This work was supported in part by the Dr. Miriam and Sheldon G. Adelson Medical Research Foundation, Center of Excellence Grant 1779/11 from the Israel Science Foundation, the Robert Bosch Stiftung Foundation, the German–Israeli Foundation for Scientific Research, the Moross Integrated Cancer Center, and the Estate of John Hunter. S.V.'s contribution was partially supported by the Croatian Science Foundation. M.O. holds the Andre Lwoff chair in molecular biology.

1. Bartel DP (2004) MicroRNAs: Genomics, biogenesis, mechanism, and function. *Cell* 116(2):281–297.
2. Baskerville S, Bartel DP (2005) Microarray profiling of microRNAs reveals frequent coexpression with neighboring miRNAs and host genes. *RNA* 11(3):241–247.
3. Kim Y-K, Kim VN (2007) Processing of intronic microRNAs. *EMBO J* 26(3):775–783.
4. Hu W, et al. (2010) Negative regulation of tumor suppressor p53 by microRNA miR-504. *Mol Cell* 38(5):689–699.
5. Bieging KT, Mello SS, Attardi LD (2014) Unravelling mechanisms of p53-mediated tumour suppression. *Nat Rev Cancer* 14(5):359–370.
6. Levine AJ, Oren M (2009) The first 30 years of p53: Growing ever more complex. *Nat Rev Cancer* 9(10):749–758.
7. Vousden KH, Prives C (2009) Blinded by the light: The growing complexity of p53. *Cell* 137(3):413–431.
8. Olsen SK, et al. (2003) Fibroblast growth factor (FGF) homologous factors share structural but not functional homology with FGFs. *J Biol Chem* 278(36): 34226–34236.
9. Schoorlemmer J, Goldfarb M (2001) Fibroblast growth factor homologous factors are intracellular signaling proteins. *Curr Biol* 11(10):793–797.
10. Zhang X, Bao L, Yang L, Wu Q, Li S (2012) Roles of intracellular fibroblast growth factors in neural development and functions. *Sci China Life Sci* 55(12): 1038–1044.
11. Smallwood PM, et al. (1996) Fibroblast growth factor (FGF) homologous factors: New members of the FGF family implicated in nervous system development. *Proc Natl Acad Sci USA* 93(18):9850–9857.
12. Goldfarb M (2005) Fibroblast growth factor homologous factors: Evolution, structure, and function. *Cytokine Growth Factor Rev* 16(2):215–220.
13. Greene JM, et al. (1998) Identification and characterization of a novel member of the fibroblast growth factor family. *Eur J Neurosci* 10(5):1911–1925.
14. Gecz J, et al. (1999) Fibroblast growth factor homologous factor 2 (FHF2): Gene structure, expression and mapping to the Börjeson-Forssman-Lehmann syndrome region in Xq26 delineated by a duplication breakpoint in a BFLS-like patient. *Hum Genet* 104(1):56–63.
15. Munoz-Sanjuan I, Smallwood PM, Nathans J (2000) Isoform diversity among fibroblast growth factor homologous factors is generated by alternative promoter usage and differential splicing. *J Biol Chem* 275(4):2589–2597.
16. Hoek K, et al. (2004) Expression profiling reveals novel pathways in the transformation of melanocytes to melanomas. *Cancer Res* 64(15):5270–5282.
17. Missiaglia E, et al. (2010) Pancreatic endocrine tumors: Expression profiling evidences a role for AKT-mTOR pathway. *J Clin Oncol* 28(2):245–255.
18. Levy C, et al. (2010) Intronic miR-211 assumes the tumor suppressive function of its host gene in melanoma. *Mol Cell* 40(5):841–849.
19. Najafi-Shoushtari SH, et al. (2010) MicroRNA-33 and the SREBP host genes cooperate to control cholesterol homeostasis. *Science* 328(5985):1566–1569.
20. Gao X, Qiao Y, Han D, Zhang Y, Ma N (2012) Enemy or partner: Relationship between intronic micrornas and their host genes. *IUBMB Life* 64(10):835–840.
21. Luo J, Solimini NL, Elledge SJ (2009) Principles of cancer therapy: Oncogene and non-oncogene addiction. *Cell* 136(5):823–837.
22. Cerami E, et al. (2012) The cBio cancer genomics portal: An open platform for exploring multidimensional cancer genomics data. *Cancer Discov* 2(5):401–404.
23. Gasparini P, et al. (2015) microRNA classifiers are powerful diagnostic/prognostic tools in ALK-, EGFR-, and KRAS-driven lung cancers. *Proc Natl Acad Sci USA* 112(48): 14924–14929.
24. Wu QF, et al. (2012) Fibroblast growth factor 13 is a microtubule-stabilizing protein regulating neuronal polarization and migration. *Cell* 149(7):1549–1564.
25. Wang C, et al. (2011) Fibroblast growth factor homologous factor 13 regulates Na+ channels and conduction velocity in murine hearts. *Circ Res* 109(7):775–782.
26. Scott MS, Boisvert FM, McDowall MD, Lamond AI, Barton GJ (2010) Characterization and prediction of protein nucleolar localization sequences. *Nucleic Acids Res* 38(21): 7388–7399.
27. Scott MS, Troshin PV, Barton GJ (2011) NoD: A nucleolar localization sequence detector for eukaryotic and viral proteins. *BMC Bioinformatics* 12:317.
28. Yung BY, Bor AM, Chan PK (1990) Short exposure to actinomycin D induces "reversible" translocation of protein B23 as well as "reversible" inhibition of cell growth and RNA synthesis in HeLa cells. *Cancer Res* 50(18):5987–5991.
29. Derenzini M, et al. (1998) Nucleolar function and size in cancer cells. *Am J Pathol* 152(5):1291–1297.
30. Kim HJ, et al. (2011) Systemic analysis of heat shock response induced by heat shock and a proteasome inhibitor MG132. *PLoS One* 6(6):e20252.
31. Khalouei S, Chow AM, Brown IR (2014) Localization of heat shock protein HSPA6 (HSP70B′) to sites of transcription in cultured differentiated human neuronal cells following thermal stress. *J Neurochem* 131(6):743–754.
32. Milyavsky M, et al. (2003) Prolonged culture of telomerase-immortalized human fibroblasts leads to a premalignant phenotype. *Cancer Res* 63(21):7147–7157.
33. Milyavsky M, et al. (2005) Transcriptional programs following genetic alterations in p53, INK4A, and H-Ras genes along defined stages of malignant transformation. *Cancer Res* 65(11):4530–4543.
34. Aylon Y, et al. (2009) Silencing of the Lats2 tumor suppressor overrides a p53-dependent oncogenic stress checkpoint and enables mutant H-Ras-driven cell transformation. *Oncogene* 28(50):4469–4479.
35. Kanies CL, et al. (2008) Oncogenic Ras and transforming growth factor-beta synergistically regulate AU-rich element-containing mRNAs during epithelial to mesenchymal transition. *Mol Cancer Res* 6(7):1124–1136.
36. Bellot GL, Liu D, Pervaiz S (2013) ROS, autophagy, mitochondria and cancer: Ras, the hidden master? *Mitochondrion* 13(3):155–162.
37. Gao W, et al. (2011) MiR-21 overexpression in human primary squamous cell lung carcinoma is associated with poor patient prognosis. *J Cancer Res Clin Oncol* 137(4): 557–566.
38. Yang MH, et al. (2012) Connective tissue growth factor modulates oral squamous cell carcinoma invasion by activating a miR-504/FOXP1 signalling. *Oncogene* 31(19): 2401–2411.
39. Soutto M, et al. (2014) TFF1 activates p53 through down-regulation of miR-504 in gastric cancer. *Oncotarget* 5(14):5663–5673.
40. Jiang B, Gu Y, Chen Y (2014) Identification of novel predictive markers for the prognosis of pancreatic ductal adenocarcinoma. *Cancer Invest* 32(6):218–225.
41. Ford NA, Dunlap SM, Wheatley KE, Hursting SD (2013) Obesity, independent of p53 gene dosage, promotes mammary tumor progression and upregulates the p53 regulator microRNA-504. *PLoS One* 8(6):e68089.
42. Scoccianti C, et al.; European Early Lung Cancer Consortium (2012) Prognostic value of TP53, KRAS and EGFR mutations in nonsmall cell lung cancer: The EUELC cohort. *Eur Respir J* 40(1):177–184.
43. Rickards B, Flint SJ, Cole MD, LeRoy G (2007) Nucleolin is required for RNA polymerase I transcription in vivo. *Mol Cell Biol* 27(3):937–948.
44. Okada T, et al. (2013) Upregulated expression of FGF13/FHF2 mediates resistance to platinum drugs in cervical cancer cells. *Sci Rep* 3:2899.
45. Krejci P, Mekikian PB, Wilcox WR (2006) The fibroblast growth factors in multiple myeloma. *Leukemia* 20(6):1165–1168.
46. Budde A, Grummt I (1999) p53 represses ribosomal gene transcription. *Oncogene* 18(4):1119–1124.
47. Sugimoto M, Kuo ML, Roussel MF, Sherr CJ (2003) Nucleolar Arf tumor suppressor inhibits ribosomal RNA processing. *Mol Cell* 11(2):415–424.
48. Dai C, Whitesell L, Rogers AB, Lindquist S (2007) Heat shock factor 1 is a powerful multifaceted modifier of carcinogenesis. *Cell* 130(6):1005–1018.
49. Dey S, Tameire F, Koumenis C (2013) PERK-ing up autophagy during MYC-induced tumorigenesis. *Autophagy* 9(4):612–614.
50. Croft A, et al. (2014) Oncogenic activation of MEK/ERK primes melanoma cells for adaptation to endoplasmic reticulum stress. *J Invest Dermatol* 134(2):488–497.
51. Deshaies RJ (2014) Proteotoxic crisis, the ubiquitin-proteasome system, and cancer therapy. *BMC Biol* 12:94.
52. Sherman MY, Qian S-B (2013) Less is more: Improving proteostasis by translation slow down. *Trends Biochem Sci* 38(12):585–591.
53. Dufey E, Urra H, Hetz C (2015) ER proteostasis addiction in cancer biology: Novel concepts. *Semin Cancer Biol* 33:40–47.
54. Shah SP, Lonial S, Boise LH (2015) When cancer fights back: Multiple myeloma, proteasome inhibition, and the heat-shock response. *Mol Cancer Res* 13(8):1163–1173.
55. Wang J, et al. (2013) PHF6 regulates cell cycle progression by suppressing ribosomal RNA synthesis. *J Biol Chem* 288(5):3174–3183.
56. Cai X, et al. (2015) Runx1 deficiency decreases ribosome biogenesis and confers stress resistance to hematopoietic stem and progenitor cells. *Cell Stem Cell* 17(2):165–177.
57. Meacham CE, et al. (2015) A genome-scale in vivo loss-of-function screen identifies Phf6 as a lineage-specific regulator of leukemia cell growth. *Genes Dev* 29(5): 483–488.
58. Sablina AA, et al. (2005) The antioxidant function of the p53 tumor suppressor. *Nat Med* 11(12):1306–1313.
59. Alexandrova EM, et al. (2015) Improving survival by exploiting tumour dependence on stabilized mutant p53 for treatment. *Nature* 523(7560):352–356.
60. Hoffman Y, Bublik DR, Pilpel Y, Oren M (2014) miR-661 downregulates both Mdm2 and Mdm4 to activate p53. *Cell Death Differ* 21(2):302–309.
61. Golomb L, et al. (2012) Importin 7 and exportin 1 link c-Myc and p53 to regulation of ribosomal biogenesis. *Mol Cell* 45(2):222–232.
62. Andersen JS, et al. (2002) Directed proteomic analysis of the human nucleolus. *Curr Biol* 12(1):1–11.
63. Sulic S, et al. (2005) Inactivation of S6 ribosomal protein gene in T lymphocytes activates a p53-dependent checkpoint response. *Genes Dev* 19(24):3070–3082.
64. Guzmán C, Bagga M, Kaur A, Westermarck J, Abankwa D (2014) ColonyArea: An ImageJ plugin to automatically quantify colony formation in clonogenic assays. *PLoS One* 9(3):e92444.
65. Li G-Z, et al. (2009) Database searching and accounting of multiplexed precursor and product ion spectra from the data independent analysis of simple and complex peptide mixtures. *Proteomics* 9(6):1696–1719.
66. Levin Y, Hradetzky E, Bahn S (2011) Quantification of proteins using data-independent analysis (MSE) in simple and complex samples: A systematic evaluation. *Proteomics* 11(16):3273–3287.
67. Silva JC, Gorenstein MV, Li G-Z, Vissers JPC, Geromanos SJ (2006) Absolute quantification of proteins by LCMSE: A virtue of parallel MS acquisition. *Mol Cell Proteomics* 5(1):144–156.
68. Kim D, et al. (2013) TopHat2: Accurate alignment of transcriptomes in the presence of insertions, deletions and gene fusions. *Genome Biol* 14(4):R36.
69. Anders S, Pyl PT, Huber W (2015) HTSeq–a Python framework to work with high-throughput sequencing data. *Bioinformatics* 31(2):166–169.
70. Anders S, Huber W (2010) Differential expression analysis for sequence count data. *Genome Biol* 11(10):R106.
71. van Schadewijk A, van't Wout EFA, Stolk J, Hiemstra PS (2012) A quantitative method for detection of spliced X-box binding protein-1 (XBP1) mRNA as a measure of endoplasmic reticulum (ER) stress. *Cell Stress Chaperones* 17(2):275–279.